Post-print of: Coll, M. et al. “Beneficial effects of IL-37 after spinal cord injury in mice” in PNAS, vol. 113, issue 5 (2016), p. 1411-1416. The final version is available at DOI 10.1073/pnas.1523212113

Beneficial effects of IL-37 After Spinal Cord Injury in Mice

Marina Coll-Miró[1], Isaac Francos-Quijorna[1], Eva Santos-Nogueira[1], Abel Torres-Espin[1], Philip Bufler[2], Charles A Dinarello[3,4*] and Rubèn Lopez-Vales[1*]

[1]Departament de Biologia Cel·lular, Fisiologia i Immunologia, Institut de Neurociències, Centro de Investigación Biomédica en Red sobre Enfermedades Neurodegenerativas (CIBERNED), Universitat Autònoma de Barcelona, Bellaterra, 08193 Catalonia Spain; [2]Department of Pediatrics, Dr. von Hauner Children's Hospital Ludwig-Maximilians-University, Munich, D-80337 Munich Germany; [3]Division of Infectious Diseases, University of Colorado Denver, Aurora, CO 80045; [4]Department of Medicine, Radboud University Medical Center, Nijmegen, The Netherlands.

Short title: IL-37 in SCI

Classification: Biological Science, Neuroscience

Keywords: Interleukin-37, Spinal Cord Injury, Inflammation, Neuroprotection

***Corresponding author:** To whom correspondence may be addressed. E-mail: cdinarello@mac.com or ruben.lopez@uab.cat

ABSTRACT

Interleukin 37 (IL-37), a member of the IL-1 family, broadly reduces innate inflammation as well as acquired immunity. However, it remains unknown whether the anti-inflammatory properties of IL-37 include the central nervous system. In the present study, we subjected mice to spinal cord compression injuries. We compared mice that are transgenic for human IL-37 (hIL-37tg) to wild-type (WT) mice; we also treated WT mice with recombinant IL-37. In hIL-37tg mice, the expression of IL-37 was barely detectable in the uninjured cords, but strongly induced 24 and 72 hours after the injury. Compared to WT mice, hIL-37tg mice exhibited increased myelin and neuronal sparing and protection against locomotor deficits including a 2.5 fold greater speed under forced treadmill challenge. Reduced levels of cytokines, such as an 80% reduction in IL-6, were observed in the injured cords of hIL-37tg mice, as well as, lower numbers of blood-borne neutrophils, macrophages and activated microglia. We treated WT mice with single intraspinal injection of either full-length or processed recombinant IL-37 after the injury. We observed that IL-37-treated mice had significantly enhanced locomotor skills in an open field using the BMS score test, as well as, supported faster speed on a mechanical treadmill. Both forms of recombinant IL-37 led to similar beneficial effects on locomotor recovery after the injury. Overall, this study presents novel data indicating that IL-37 suppresses inflammation in a clinically relevant model of spinal cord injury, and concludes that recombinant IL-37 may have therapeutic potential for the treatment of acute spinal cord injuries.

Significance Statement

Spinal cord injuries often result in severely impaired locomotor, sensory and autonomic function. Although inflammation contributes to the physiopathology of spinal cord injury, several clinical trials of high doses of dexamethasone or methylprednisolone have not resulted in improved recovery of function. IL-37, a member of the IL-1 family, exerts broad anti-inflammatory effects in several mouse models of inflammatory diseases. We report here that mice expressing human IL-37 exhibit reduced inflammation in the central nervous system and resulted in significantly improved functional disabilities following spinal cord injury. The administration of recombinant forms of human IL-37 enhances motor skills after spinal cord injury, suggesting that IL-37 could provide a new therapeutic approach to limit the harmful effects of inflammation in neurological conditions.

\body

INTRODUCTION

The inflammatory response plays an essential role in protecting after injury or invasion by microorganisms (1, 2). Regardless of the tissue, unless regulated, inflammation can become chronic and result in tissue damage and loss of function (1, 2). This is particularly the case of spinal cord injury. After spinal cord contusion or compression injury, there is a rapid initiation of inflammation in rodents and in humans (2). This response is orchestrated by endogenous microglial cells, and by circulating leukocytes, especially monocytes and neutrophils, which invade the lesion site during the first hours and days following injury (2-4). Although these cells are required for the clearance of cellular and myelin debris, they also release cytokines and cytotoxic

factors, which are harmful to neurons, glia, axons and myelin, resulting in secondary damage to adjacent regions of the spinal cord that had been previously unaffected by the insult (2, 5, 6). Indeed, it is currently well accepted that inflammation is a major contributor to secondary cell death after spinal cord injury (SCI). The damaging effects of inflammation are more pronounced in the central nervous system (CNS) than in other tissues because of the limited capacity for axon regeneration and replenishment of damaged neurons and glial cells, which leads to irreversible functional disabilities (7, 8). Therefore, targeting inflammation is a valuable approach to promote neuroprotection and limit functional deficits in SCI.

Cytokines are key players in the initiation, progression and suppression of inflammation. Although several members of the interleukin-1 (IL-1) family are pro-inflammatory (9, 10), IL-37 has broad suppressive effects on innate inflammation and acquired immunity (11-14). Since a complete open reading frame for the mouse homolog of IL-37 has not been found, it was necessary to generate a strain of transgenic mice expressing human IL-37 (hIL-37tg mice). These mice are protected against endotoxin shock, colitis, hepatitis and myocardial infarction (9, 13, 15-18). However, a role for IL-37 after CNS trauma remains unexplored. In the current study, we subjected hIL-37tg to SCI and studied subsequent functional impairments in comparison to wild type (WT) mice. We also administered recombinant IL-37 to WT mice in order to provide a rationale for clinical use of IL-37 as a therapeutic. We provide direct evidence for the first time that IL-37 exerts marked anti-inflammatory properties for the contused spinal cord, and confers protection from tissue damage and functional loss.

RESULTS

hIL-37tg mice exhibit reduced functional deficits and tissue damage after SCI

As shown in Figure 1A, hIL-37tg mice displayed significant improvement in locomotor recovery after SCI. There were significant improvements in BMS scores starting at day 7 after injury, and remaining significantly enhanced for the following 3 weeks (Fig. 1A). At the 28th day post-injury (dpi), all WT mice showed extensive ankle movement, but only 50% of these mice showed plantar paw placement but no weight-bearing stepping (BMS score 2.5). In contrast, all hIL-37tg mice showed extensive ankle movement, plantar paw placement with weight support, and the majority displayed occasional stepping (BMS score 3.8) (Fig. 1A). Moreover, hIL-37tg mice performed ~2.5 fold faster locomotion on the treadmill than WT mice (Fig. 1B), further demonstrating the protective effect of IL-37 against functional loss in SCI.

We then assessed whether the improvement in motor skills of hIL-37tg mice was associated with reduced secondary tissue damage after SCI. Histological sections from the injury epicenter stained with luxol fast blue (LFB) revealed enhanced myelin sparing in hIL-37tg compared to WT mice (Fig 1C, D). Prevention of myelin loss by transgenic expression of IL-37 was evident at the lesion epicenter and at distances up to 800 μm caudal to the injury (Fig 1C, D). Assessment of neuronal sparing in the ventral horns also demonstrated attenuated neuronal loss in hIL-37tg (Fig. 1E, F). Spinal cord sections stained against NeuN revealed that hIL-37tg mice had greater numbers of neurons at several regions rostral and caudal to the injury epicenter in hIL-37tg mice (Fig. 1 E, F).

Since infiltrating macrophages inhibit axonal outgrowth by releasing soluble factors and by cell-cell interaction (19, 20), we sought to evaluate whether there was enhanced axonal regeneration in hIL-37tg mice after complete spinal cord transection. hIL-37tg and WT mice presented complete hindlimb paralysis after the injury and lacked functional improvement at 10 weeks post-lesion (BMS score 0). Histological

assessment of sagittal spinal cord tissue sections revealed that transgenic expression of IL-37 did not led to regeneration of axons beyond the transection site. Similarly, axonal counts at rostral distances to the injury did not reveal any difference between hIL-37tg and WT mice (Fig. 2), suggesting that IL-37 did not promote regeneration/sprouting of corticospinal axons (Fig. 2). Overall, these data provide evidence that IL-37 confers protection from functional disabilities and secondary tissue damage after spinal cord contusion injury, but does not promote axonal outgrowth of the corticospinal tract.

IL-37 is induced in hIL-37tg mice after SCI

Since hIL-37tg mice were markedly protected against functional disabilities and tissue loss after SCI, we studied the inflammatory response in hIL-37tg mice. We first assessed the expression profile of IL-37 in the spinal cord of hIL-37tg mice determined by PCR. Expectedly, IL-37 was not present in the intact or damaged spinal cord obtained from WT mice. hIL-37tg mice exhibited a low level of constitutive expression of IL-37 in the spinal cord. Low levels of constitutive IL-37 expression in the transgenic mice have also been observed in the colon, skin, circulating leukocytes or in cell lines transfected with IL-37 (11, 13, 16). The low levels are due to the instability sequence in human IL-37 (14). However, after the contusion injury, induction of IL-37 in the spinal cord parenchyma was observed (Fig. 3). IL-37 expression profile occurred at 2 peaks of expression; after 12 hours and at day 3 post-injury, when the levels of IL-37 increased ~17 and ~35 fold, respectively (Fig. 3). The early peak of IL-37 coincides with the induction of cytokines in the injured spinal cord 6-24 hours post-injury (Fig. S1 and Fig. S2), whereas the latter correlates with the infiltration of blood monocytes (day 3) (2).

Inhibition of cytokine and chemokine expression after SCI

We next sought to examine whether the early increase in IL-37 modulated gene expression of cytokines in the contused spinal cord. Injured spinal cords harvested at 12 and 24 hours post-contusion, which are time periods when the protein levels of most cytokines and chemokines reach maximal concentrations after SCI (2). We evaluated the protein levels of 32 cytokines in the injured spinal cord. At 12 hours post-injury, cytokine levels were unchanged in hIL-37tg relative to WT mice (Fig. S2). However, at 24 hours post-injury, we observed a significant reduction in the expression of 23 out of the 32 cytokines in hIL-37tg mice (Fig. S1). Moreover, the expression of IL-3, which was detected at low levels in the spinal cord homogenates of WT mice (0.56±0.03 pg/mg protein), was undetectable in hIL-37tg mice (<0.45 pg/mg protein). The levels of 6 cytokines (LIF, M-CSF, IL-2, IL-5, IL-15, and eotaxin) did not change in IL-37tg mice, whereas the expression of IL-4, IL-12p40 was not detected in the contused spinal cord of both experimental groups (Fig. S1).

We next evaluated the accumulation of inflammatory cells between WT mice and hIL-37tg mice following SCI. At day 1 post-injury, when granulocyte infiltration reaches peak levels, the spinal cord of hIL-37tg mice showed ~40% reduction in the number of granulocytes (Fig. 4). There were no differences in the cell counts for activated microglia, blood borne macrophages, CD4 and CD8 T cell, at this time point (Fig. 4).

Seven days post-injury, when the accumulation of activated microglia and macrophages reaches peak levels in the injured spinal cord and accounts for ~80% of total immune cells, spinal cords from hIL-37tg mice exhibited significantly lower numbers of these two cell subsets (Fig. 5). The number of granulocytes, which were reduced by 90% compared to day 1, were slightly increased in hIL-37tg, but did not

reach statistical significance, whereas counts for CD4 and CD8 lymphocytes were unchanged (Fig. 3). We also assessed whether IL-37 modulated macrophage and microglia polarization after SCI. However, FACS analysis from contused spinal cords revealed no differences in IL-37tg mice for the expression of CD16/32 and CD206 on microglia (CD16/32: 76.2±4.2 vs 74.6±3.8; CD206: 14,1±3.1 vs 15.2±3.1 in WT and IL37tg, respectively) or macrophages (CD16/32 82.2±6.7 vs 79.4±5.3; CD206 14.5±1.9 vs 16.6±3.2 in WT and IL-37tg, respectively), two known markers of M1 and M2 activation, respectively.

Intralesional administration of recombinant IL-37 improves functional outcomes after SCI

To assess a therapeutic use of IL-37 in SCI, we administered recombinant forms of human IL-37 (rlL-37) to determine possible beneficial effects in SCI. We first tested the IL-37 precursor (full-length of IL-37 isoform b), as previous studies have shown efficacy *in vivo* (21) and *in vitro* (22). We also administered a processed form of IL-37 with the N-terminus at valine 46 (22, 23). Since the blood brain barrier prevents the entry of most molecules into the CNS, we infused rIL-37 into the lesion site 5 minutes after contusion injury, using a glass capillary (30µm diameter). As shown in Fig. 6A, intraspinal injection of either full-length or processed rIL-37 significantly enhanced locomotor recovery in the BMS score, starting at day 10 post-injury. At day 28, mice injected with saline had a BMS score of 1.6, which corresponds to slight or extensive movement of the ankle. However, treatment with full-length rIL-37 improved the BMS score in 1 point (Fig. 6A). rIL-37-treated mice showed extensive movement of the ankle and most of them also displayed plantar paw placement in at least one paw, but no stepping. Moreover, treatment with full-length rIL-37 increased in 50% the speed that

mice were able to achieve on a treadmill (Fig. 6B), further suggesting the beneficial effects of rIL-37 in preventing functional deficits after SCI. Overall, both forms of rIL-37 led to similar beneficial effects on motor skills (Fig. 6).

DISCUSSION

Although IL-37 is lacking in mice, hIL-37tg mice are protected against several inflammatory challenge. Using the hIL-37tg mouse, previous studies have consistently demonstrated the suppressive properties of IL-37 on inflammation (11, 13, 16). However, whether IL-37 exerts a similar anti-inflammatory effect in the CNS trauma remained unknown. Here we demonstrate for the first time that IL-37 suppresses inflammation and limits locomotor deficits and tissue damage in spinal cord contusion injury in the mouse. This conclusion is based on observations in IL-37tg mice as well as in WT mice treated with either recombinant IL-37 precursor or processed IL-37.

In hIL-37tg mice, the expression is regulated by a constitutive cytomegalovirus (CMV) promoter (13) and thus, it should induce the expression in all cells. However, constitutive expression of IL-37 in the spinal cord is low owing to the presence of an instability sequence that limits the half-life of the IL-37 transcript (14). This has been also shown in other models using these mice (11, 13, 16). However, upon inflammatory conditions, such as the trauma to tissue, there is activation of inflammatory components, which increases the half-life of IL-37 mRNA and allows for translation of the protein IL-37. IL-37 mRNA stability is apparently regulated by instability elements present in exon 5, as exon 5 deletion can significantly increase mRNA stability of both IL-37b and IL-37c. A similar mRNA stabilization upon LPS stimulation can be observed for IL-18 (14). We observed that mRNA levels were induced 12 hours after SCI and then a secondary increase occurs 3 days after the injury. It remains unknown, however,

whether endogenous IL-37 is expressed in human SCI. Cytokines such as IL-1β, TLR agonist and TGFβ are known to induce IL-37 in vitro (13). Cytokine expression reaches maximal levels in the spinal cord within 6-24 hours post-injury (2), which may account for the first peak of IL-37. Although IL-37 is mainly expressed in macrophages in hIL-37tg mice after several inflammatory challenges (13, 16, 24), endogenous glial cells (astrocytes and microglia) are probably the early source of IL-37 due to the low amount of infiltrated leukocytes at this time point. However, the later expression peak of IL-37 (3dpi) coincides with the entrance of blood borne monocytes into the spinal cord, suggesting that macrophages are the main source of the second peak of IL-37 (2).

IL-37 reduces the expression of several pro-inflammatory cytokines in cell cultures and in different inflammatory disorders (13, 15, 16, 18, 25). We also found that IL-37 attenuated the protein levels of most pro-inflammatory cytokines evaluated in contused spinal cord, IL-6 being most markedly effected. The capacity of IL-37 to reduce cytokine production after SCI impacted on the infiltration and activation of immune cells. Indeed, IL-37 reduced the recruitment of neutrophils and macrophages into the injured spinal cord, but also the activation state of the microglia. However, IL-37 did not affect the infiltration of T cells.

Regardless of the species or type of SCI, anti-inflammatories or myeloid cell depletion consistently reveal reduced tissue damage and greater functional outcomes (2, 3). Here we show that hIL-37tg mice exhibited enhanced locomotor function that was associated with attenuated tissue damage after SCI. Blood borne monocytes infiltrating into the injured spinal cord mediate axonal retraction (19, 20) and this deleterious effect is due products released by macrophages or by integral macrophage membrane proteins, which inhibit the growth and guidance of axons (19, 20). Other inhibitory molecules include chondroitin sulphate proteoglycans, Nogo, Ephrins and semaphorins, which are

expressed at the lesion site by astrocytes, oligodendrocytes and some precursor cells (7). There is also a limited ability of adult CNS neurons to switch on the intrinsic regeneration machinery after axotomy (26). However, despite reduced macrophage numbers in spinal cords of hIL-37tg mice, axonal outgrowth was not observed, as these other factors, which hamper the ability of axons to regenerate in the injured CNS, may not be altered in the IL-37tg mouse. Therefore, our data indicate that attenuation of inflammation in the IL-37tg mouse did not overcome the extrinsic and intrinsic factors that curtail the relatively limited regenerative potential of injured corticospinal axons. It is possible that increasing the dosing of recombinant IL-37 could enhance axonal outgrowth of other motor or sensory tracts with better regeneration capabilities.

Once synthesized following activation, up to 30% of the IL-37 precursor is cleaved intracellularly by activated caspase-1 and translocates to the nucleus, most likely in association with Smad3 (13, 17). Indeed, the anti-inflammatory effects of IL-37 are abolished in LPS-stimulated macrophages when incubated with caspase-1 inhibitors, or when the caspase-1 site (D20) is mutated, and cannot translocate to the nucleus (27). Similarly, *in vivo* studies also reveal that the anti-inflammatory actions of IL-37 are lost when Smad3 is silenced after LPS challenge (13).

On the other hand, the precursor form of IL-37 is released from human monocytes, or cell lines transfected with IL-37 following LPS stimulation (13). The release of IL-37 is, however, independent on caspase-1 cleavage at D20 (27). The administration of neutralizing antibodies against IL-37 enhances cytokine production in *in vitro* and *in vivo*, highlighting the extracellular anti-inflammatory function of IL-37 (22, 27). These observations are further supported by studies showing the ability of recombinant IL-37 protein to reduce cytokine production (22). Extracellular IL-37 carries out its anti-inflammatory actions by recruiting the decoy IL-1R8 to the

IL-18Rα/IL-37 complex (28-30). Administration of recombinant IL-37 improves functional recovery after SCI, indicating that extracellular IL-37 is sufficient for its beneficial effects in the CNS. Nevertheless, we cannot rule-out the possibility that the translocation of IL-37 to the nucleus is also playing a role in the transgenic mouse and also in the human.

It is likely that processing of the IL-37 precursor appears to take place extracellularly. Edman degradation of supernatants from cells lines transfected with IL-37b revealed a processed form starting at valine 46 (IL-$37_{V46\text{-}218}$) (23). Both full length and processed IL-37 exhibit anti-inflammatory effects (22). We observed that both IL-37 forms exert similar beneficial effects on functional outcomes after SCI, suggesting that the IL−37 precursor may be processed when administered in the injured spinal cord.

In summary, recombinant IL-37 prevents functional deficits and secondary tissue damage in SCI suggesting a potential clinical application. This is the first report suggesting that IL-37 could be an effective therapy during the acute phase after SCI, for which there is currently no effective treatment.

MATERIALS AND METHODS

Animals. Experiments were performed in adult (8-10 weeks) female mice expressing the human form of IL-37 (hIL-37tg) or C57Bl/6 mice (Charles River). After SCI, motor skills were assessed in hIL-37tg mice, WT and WT mice treated with recombinant human IL-37 (r-IL-37). SI contains details about SCI models, r-IL-37 delivery, and functional assessment.

Tissue processing. Spinal cords were cut on a cryostat and stained for assessing neuron survival, myelin sparing and axonal regeneration. Moreover, spinal cords were processed for RNA, cytokine protein level analysis and for FACS analysis. For more detail, see SI.

AUTHOR CONTRIBUTIONS

C.A.D. and R.L-V. designed research; M.C-M., I.F-Q., E.S-N, and R.L-V. performed research; P.B. and C.A.D. contributed new reagents/analytic tools; M.C-M., C.A.D., and R.L-V. analyzed data; M.C-M., C.A.D., and R.L-V. wrote the paper.

ACKNOWLEGMENTS

This work was supported by grants from Fundació La Marató, Spanish Ministry of Economy and Competitiveness (SAF2013-48431-R), International Foundation for Research in Paraplegia, and by funds from the Fondo de Investigación Sanitaria of Spain (TERCEL and CIBERNED) to R.L-V. The studies were also supported by NIH grant AI-15614 to C.A. D., and by DFG grant BU 1222/3-3 to P.B.

REFERENCES

1. Serhan CN (2014) Pro-resolving lipid mediators are leads for resolution physiology. *Nature* 510(7503):92-101.
2. David S, Lopez-Vales R, & Wee Yong V (2012) Harmful and beneficial effects of inflammation after spinal cord injury: potential therapeutic implications. *Handbook of clinical neurology* 109:485-502.
3. Popovich PG (2014) Neuroimmunology of traumatic spinal cord injury: a brief history and overview. *Exp Neurol* 258:1-4.
4. David S, Greenhalgh AD, & Lopez-Vales R (2012) Role of phospholipase A2s and lipid mediators in secondary damage after spinal cord injury. *Cell Tissue Res* 349(1):249-267.
5. Lopez-Vales R, *et al.* (2011) Phospholipase A2 superfamily members play divergent roles after spinal cord injury. *FASEB J* 25(12):4240-4252.
6. Alexander JK & Popovich PG (2009) Neuroinflammation in spinal cord injury: therapeutic targets for neuroprotection and regeneration. *Prog Brain Res* 175:125-137.
7. Silver J, Schwab ME, & Popovich PG (2014) Central Nervous System Regenerative Failure: Role of Oligodendrocytes, Astrocytes, and Microglia. *Cold Spring Harb Perspect Biol* 7(3).
8. Rowland JW, Hawryluk GW, Kwon B, & Fehlings MG (2008) Current status of acute spinal cord injury pathophysiology and emerging therapies: promise on the horizon. *Neurosurg Focus* 25(5):E2.
9. Garlanda C, Dinarello CA, & Mantovani A (2013) The interleukin-1 family: back to the future. *Immunity* 39(6):1003-1018.

10. Dinarello CA, Simon A, & van der Meer JW (2012) Treating inflammation by blocking interleukin-1 in a broad spectrum of diseases. *Nat Rev Drug Discov* 11(8):633-652.
11. Luo Y, *et al.* (2014) Suppression of antigen-specific adaptive immunity by IL-37 via induction of tolerogenic dendritic cells. *Proc Natl Acad Sci U S A* 111(42):15178-15183.
12. Dinarello CA & Bufler P (2013) Interleukin-37. *Semin Immunol* 25(6):466-468.
13. Nold MF, *et al.* (2010) IL-37 is a fundamental inhibitor of innate immunity. *Nat Immunol* 11(11):1014-1022.
14. Bufler P, Gamboni-Robertson F, Azam T, Kim SH, & Dinarello CA (2004) Interleukin-1 homologues IL-1F7b and IL-18 contain functional mRNA instability elements within the coding region responsive to lipopolysaccharide. *Biochem J* 381(Pt 2):503-510.
15. Ballak DB, *et al.* (2014) IL-37 protects against obesity-induced inflammation and insulin resistance. *Nat Commun* 5:4711.
16. McNamee EN, *et al.* (2011) Interleukin 37 expression protects mice from colitis. *Proc Natl Acad Sci U S A* 108(40):16711-16716.
17. Bulau AM, *et al.* (2011) In vivo expression of interleukin-37 reduces local and systemic inflammation in concanavalin A-induced hepatitis. *ScientificWorldJournal* 11:2480-2490.
18. Teng X, *et al.* (2014) IL-37 ameliorates the inflammatory process in psoriasis by suppressing proinflammatory cytokine production. *J Immunol* 192(4):1815-1823.
19. Evans TA, *et al.* (2014) High-resolution intravital imaging reveals that blood-derived macrophages but not resident microglia facilitate secondary axonal dieback in traumatic spinal cord injury. *Exp Neurol* 254:109-120.

20. Horn KP, Busch SA, Hawthorne AL, van Rooijen N, & Silver J (2008) Another barrier to regeneration in the CNS: activated macrophages induce extensive retraction of dystrophic axons through direct physical interactions. *J Neurosci* 28(38):9330-9341.

21. Moretti S, *et al.* (2014) IL-37 inhibits inflammasome activation and disease severity in murine aspergillosis. *PLoS Pathog* 10(11):e1004462.

22. Li S, *et al.* (2015) Extracellular forms of IL-37 inhibit innate inflammation in vitro and in vivo but require the IL-1 family decoy receptor IL-1R8. *Proc Natl Acad Sci U S A* 112(8):2497-2502.

23. Pan G, *et al.* (2001) IL-1H, an interleukin 1-related protein that binds IL-18 receptor/IL-1Rrp. *Cytokine* 13(1):1-7.

24. Quirk S & Agrawal DK (2014) Immunobiology of IL-37: mechanism of action and clinical perspectives. *Expert Rev Clin Immunol* 10(12):1703-1709.

25. Ye L, *et al.* (2014) IL-37 inhibits the production of inflammatory cytokines in peripheral blood mononuclear cells of patients with systemic lupus erythematosus: its correlation with disease activity. *J Transl Med* 12:69.

26. Liu K, *et al.* (2010) PTEN deletion enhances the regenerative ability of adult corticospinal neurons. *Nat Neurosci* 13(9):1075-1081.

27. Bulau AM, *et al.* (2014) Role of caspase-1 in nuclear translocation of IL-37, release of the cytokine, and IL-37 inhibition of innate immune responses. *Proc Natl Acad Sci U S A* 111(7):2650-2655.

28. Yang Y, *et al.* (2015) IL-37 inhibits IL-18-induced tubular epithelial cell expression of pro-inflammatory cytokines and renal ischemia-reperfusion injury. *Kidney Int* 87(2):396-408.

29. Nold-Petry CA, *et al.* (2015) IL-37 requires the receptors IL-18Ralpha and IL-1R8 (SIGIRR) to carry out its multifaceted anti-inflammatory program upon innate signal transduction. *Nat Immunol* 16(4):354-365.

30. Lunding L, *et al.* (2015) IL-37 requires IL-18Ralpha and SIGIRR/IL-1R8 to diminish allergic airway inflammation in mice. *Allergy*.

FIGURE LEGENDS

Figure 1. hIL-37-tg mice show enhanced functional outcomes and reduced tissue damage after SCI. (A) Locomotor skills assessed in the 9-point Basso Mouse Scale (BMS) and (B) on a treadmill. (C) Myelin sparing at various distances rostral and caudal to the injury epicenter. (D) Representative micrographs showing myelin sparing at the injury epicenter in section stained against luxol fast blue from WT and hIL-37tg mice. (E) Ventral horn neuron survival at various distances rostral and caudal to the injury epicenter. (F) Representative micrographs showing sparing of ventral horn neurons in WT and hIL-37tg mice in sections stained against NeuN at 200 µm rostral to the injury epicenter. The area outlined in the box is shown in higher magnification in panels (insert). Data are expressed as mean ±SEM. (*$p<0.05$; two-ways RM-ANOVA, Bonferroni's post hoc test in A, C and D; t-test in B; n=8 per group).

Figure 2. hIL-37tg expression does not promote axonal regeneration. (A) BDA-labelled corticospinal axons at different distances to the transection site. (B-C) Low magnification images of complete transected spinal cord showing BDA-labelled corticospinal fibers in WT (B) and hIL-37tg mice (C). Lines define the transection site. L=lesion. Data are expressed as mean ±SEM. (*$p<0.05$; one-way ANOVA, Bonferroni's post hoc test; n=8 per group).

Figure 3. Expression of IL-37 after SCI. Time course of IL-37 transcripts in the spinal cord of hIL-37tg mice after contusion injury (*$p<0.05$; one-way ANOVA, Bonferroni's post hoc test; n=4 per time point).

Figure 4. Spinal cord immune cell counts at day 1 post-injury. (A-F) Representative density plots of FACS analysis showing myeloid cells and microglia (A, B), macrophages (CD45high, CD11b+, F4/80+) (C, D), and granulocytes (CD45high, CD11b+, Gr1high) (E, F) in the spinal cord of WT and hIL-37tg mice. (G) Graph showing quantification of the different immune cell populations in the injured spinal cord. Data are expressed as mean ±SEM. (*$p<0.05$; t-test; n=4 per group).

Figure 5. Recruitment of immune cells within the spinal cord at day 7 post-injury. (A-F) Representative density plots of FACS analysis showing myeloid cells and microglia (A, B), macrophages (CD45high, CD11b+, F4/80+) (C, D), and activated microglia (CD45low, CD11b+, F4/80+) (E, F) in the spinal cord of WT and hIL-37tg mice. (G) Graph showing quantification of the different immune cell populations in the injured spinal cord. Data are expressed as mean ±SEM. (*$p<0.05$ *$p<0.001$; # $p=0.001$; t-test; n=4 per group).

Figure 6. Infusion of recombinant human IL-37 promotes functional recovery after spinal cord injury. Locomotor performance of C57BL/6 mice treated with intraspinal injection of saline, full length (IL-37_{1-218}) or processed form of IL-37b (IL-$37_{V46-218}$) after spinal cord injury using the BMS score scale (A) and (B) treadmill. Data are shown as mean ±SEM. (*$p<0.05$; two-way RM-ANOVA, Bonferroni's post hoc in A and t-test in B); n=14 for saline, n=9 for rIL-37_{1-218} and rIL-$37_{V46-218)}$.

SUPPORTING INFORMATION

MATERIALS AND METHODS

Surgical procedure

All surgical procedures were approved by the Universitat Autònoma de Barcelona Animal Care Committee and followed the guidelines of the European Commission on Animal Care. Adult (8-10 weeks old) female C57BL/6 mice (Charles River) and hIL-37tg mice (13) were anesthetized with ketamine (90 mg/kg, i.m.) and xylazine (10 mg/kg, i.m.). After performing a laminectomy at the 11th thoracic vertebrae, the exposed spinal cord was contused with a force of 60 kdynes using the Infinite Horizon Impactor device (Precision Scientific Instrumentation) (31) or was completely transected using a microscalpel. At 56 days after complete spinal cord transection, corticospinal tract was labelled by injecting a 10% solution of the axonal tracer biotinylated dextran amine (BDA) in the sensory-motor cortex (32).

Administration of recombinant human IL-37 protein (b isoform) was performed intraspinally by means of a glass capillary (30 µm internal diameter, Eppendorf, Hamburg, Germany) coupled to a 10 ml Hamilton syringe (Hamilton #701, Hamilton Co, Reno, NV, USA). 1 µl of saline, saline containing 100 ng of full length (rIL-$37_{1\text{-}218}$) or recombinant human IL-$37_{V46\text{-}218}$ was injected into injured spinal cord at the lesion site 5 minutes after lesion. Injections were made at a perfusion speed of 2 µl/min controlled by an automatic injector (KDS 310 Plus, Kd Scientific, Holliston, MA, USA), and the tip of the glass capillary was maintained inside the cord tissue 3 min after each injection to avoid liquid reflux.

RNA isolation, reverse transcription and real-time PCR

Mice were perfused with sterile saline and 5mm length of uninjured spinal cord was removed. Tissue was homogenized with QIAzol lysis reagent (Qiagen) and RNA extracted using RNeasy Lipid Tissue kit (Qiagen), according to the manufacturer's protocol. RNA was treated with DNaseI (Qiagen) to eliminate genomic DNA contamination. 1 µg of obtained RNA was primed with random hexamers (Promega) and reverse transcribed using Omniscript RT kit (Qiagen). RNase inhibitor (Roche) was added (1 U/µl final concentration) to avoid RNA degradation. Glyceraldehyde 3-phosphate dehydrogenase (GAPDH) was used as a housekeeping gene

Cytokine Protein Expression

Mice were perfused with sterile saline and a 5 mm length of spinal cord centered on the lesion was collected at 12 and 24h after surgery from hIL-37tg and WT mice and snap-frozen. Spinal cords were homogenized and protein concentration was determined using the DC Protein Assay (Bio-Rad). Samples were concentrated to 4 µg/µl using MicroCon centrifugation filters (Millipore) to ensure equal amounts of protein. The protein levels of 32 cytokines and chemokines were then analyzed using the Milliplex MAP Mouse Cytokine/Chemokine magnetic bead panel (Millipore) on a Luminex (Millipore) as per manufacturers' protocol.

Flow Cytometry

Immune cells from the injured spinal cord were analyzed by flow cytometry at 1 and 7 dpi as described previously (33). Briefly, spinal cords were cut in small pieces, passed through a cell strainer of 70 µm (BD Falcon) using saline and the cell suspension was centrifuged at 300g for 10 minutes at 4ºC. The pellet was resuspended and centrifuged for a second time. Samples were divided, and cells alone and isotype-matched control samples were generated

to control for nonspecific binding of antibodies and for auto-fluorescence. The following antibodies were also purchased from eBioscience: CD45-PerCP, CD11b-PE-Cy7, Gr1-FITC, F4/80-APC or PE, CD3-FITC, CD4-APC, CD8-APC, CD19-PE. After 30 min of incubation with combinations of antibodies at 4°C, the samples were washed and fixed in 1% paraformaldehyde. The following combination of marker was used to identify activated microglia ($CD45^{low}$, $CD11b^{+}$, $F4/80^{+}$), granulocytes as ($CD45^{high}$, $CD11b^{+}$, $F4/80^{-}$, $Gr\text{-}1^{high}$), macrophages ($CD45^{high}$, $CD11b^{+}$, $F4/80^{+}$), CD4 T-Cells ($CD45^{+}$, $CD11b^{-}$, $CD3^{+}$, $CD4^{+}$) and CD8 T-Cells ($CD45^{+}$, CD11b, $CD3^{+}$, $CD8^{+}$) (31). In addition, microglia and macrophages were further differentiated based on CD16/32 and CD206 and to assess M1 and M2 polarization, respectively. Cells were analyzed using FlowJo® software on a FACSCanto flow cytometer (BD Biosciences).

Functional assessment

Locomotor recovery was evaluated at 1, 3, 5, 7, 10, 14, 21 and 28 dpi in an open-field test using the nine-point Basso Mouse Scale (BMS) (34), which was specifically developed for locomotor testing after contusion injuries in mice. The BMS analysis of hindlimb movements and coordination was performed by two independent and blinded assessors and a consensus score taken. In addition, at the end of the follow up (day 28 post-injury), the highest locomotion speed of the mice was evaluated on a belt of a motorized treadmill. Briefly, each mouse was allowed to explore the treadmill compartment for 5min, with the motor speed set to zero. Then, speed was increased 2 cm/s every 5 seconds until the animal was not able to maintain the speed. The maximum speed at which each mouse was able to achieve for 5 seconds was recorded.

Histology

At 28 days post-injury mice were perfused with 4% paraformaldehyde in 0.1M-phosphate buffer (PB) at 12h, 3 and 28 dpi. A 5mm length of spinal cord containing the lesion site was removed, cryoprotected with 30% sucrose in 0.1M PB at 4ºC, and 6 series of 10µm thick section were picked up on glass slides. Adjacent sections on the same slide were therefore 100µm apart. For demyelination analyses, sections were stained with Luxol fast blue (LFB) (Sigma). After graded dehydration, sections were placed in a 1 mg/ml LFB solution in 95% ethanol and 0.05% acetic acid overnight at 37ºC. Sections were then washed in 95% ethanol and distilled water before place them into a solution of 0.5 mg/ml Li2CO3 in distilled water for 1 min at RT. After washes in distilled water, sections were dehydrated and mounted in DPX mounting media (Sigma). For neuronal assessment, sections were incubated overnight at 4ºC with biotinylated antibodies against NeuN. After several washes in PBS, sections were stained using the ABC kit (Vector labs) then a coverslip was applied in DPX mounting media (Sigma).

The epicenter of the injection or contusion injury impact was determined for each mouse spinal cord by localizing the tissue section with the greatest damage using LFB stained section. Myelin sparing after SCI was calculated by delineating the spared LFB stained tissue area from images taken at x40 magnification at the injury epicenter, and every 200 µm rostral and caudal to the lesion site. Neuronal survival was assessed by manually counting the number of $NeuN^+$ cells in high magnification (x400) images taken from the both ventral horns at the injury epicenter and very 200 µm rostral and caudal to the lesion site. The NIH ImageJ software was used to quantify all these histological parameters.

10 days after BDA tracer injections (66 days post-injury) mice were perfused, and the transected spinal cord harvested and cut on 20 µm thick sagittal sections as described above. Visualization of corticospinal fibers of done by incubating the spinal cord sections with Alexa

594-conjugated streptavidin. Pictures from the spinal cord covering the transection lesion and up 3000 µm rostral were taken at x200 magnification, and then merged into collages using the Photoshop software. Only sections that contained BDA-labeled fibers were acquired. The number of pixels of BDA-labeled fibers with a dorso-ventral line was counted every 150 µm over the rostro-caudal axis using NIH software.

FIGURES

Fig. S1. Multiplex analysis of cytokine protein profiles from spinal cord of WT and hIL-37tg mice at 24 hours post-injury. Data are expressed as fold change vs WT mice (mean ±SEM).

Fig. S2. Multiplex analysis of cytokine protein profiles from spinal cord of WT and hIL-37tg mice at 12 hours post-lesion. Data are expressed as fold change vs WT mice (mean ±SEM).

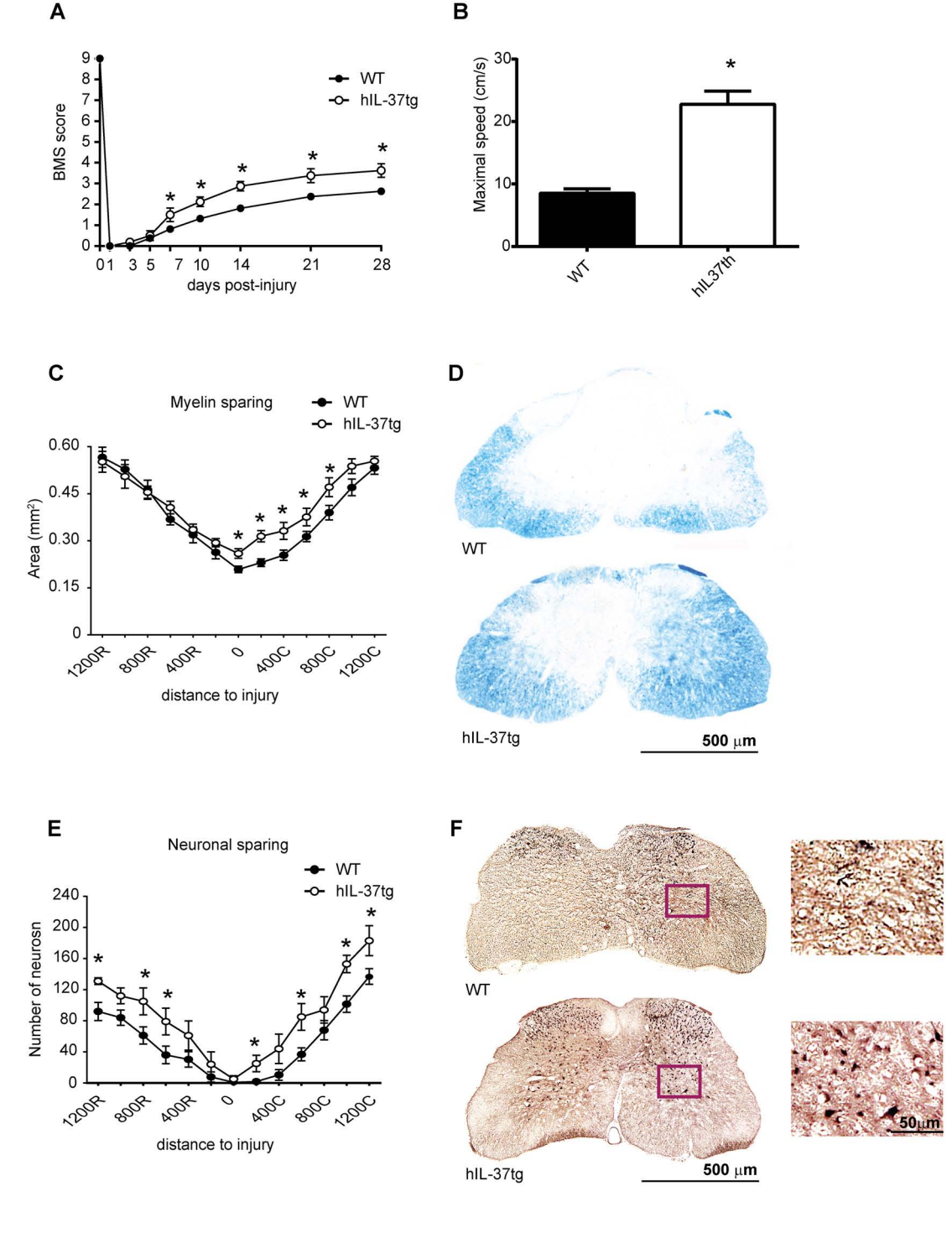
A
BMS score
WT
hIL-37tg
days post-injury
B
Maximal speed (cm/s)
WT
hIL37th
C
Myelin sparing
WT
hIL-37tg
Area (mm²)
distance to injury
D
WT
hIL-37tg
500 μm
E
Neuronal sparing
WT
hIL-37tg
Number of neurosn
distance to injury
F
WT
hIL-37tg
500 μm
50μm

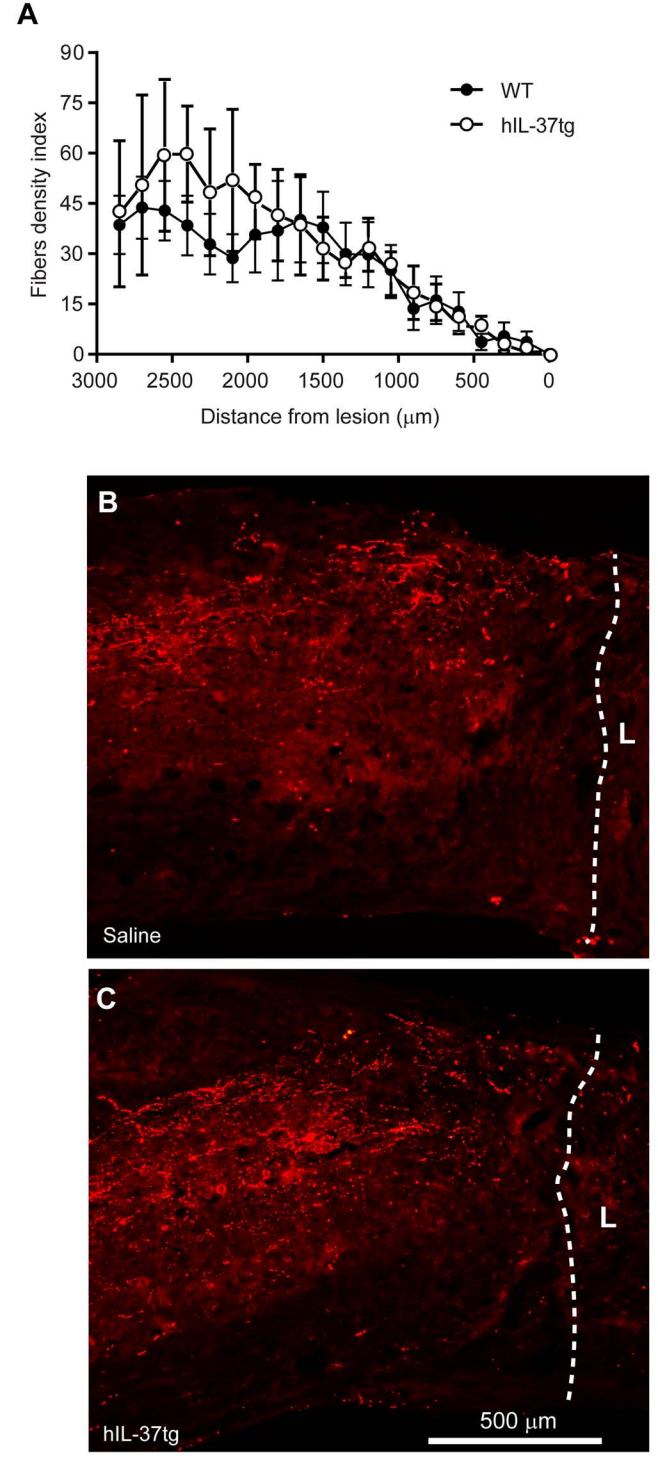
A
90
75
60
45
30
15
0
Fibers density index
WT
hIL-37tg
3000
2500
2000
1500
1000
500
0
Distance from lesion (μm)
B
L
Saline
C
L
hIL-37tg
500 μm

A

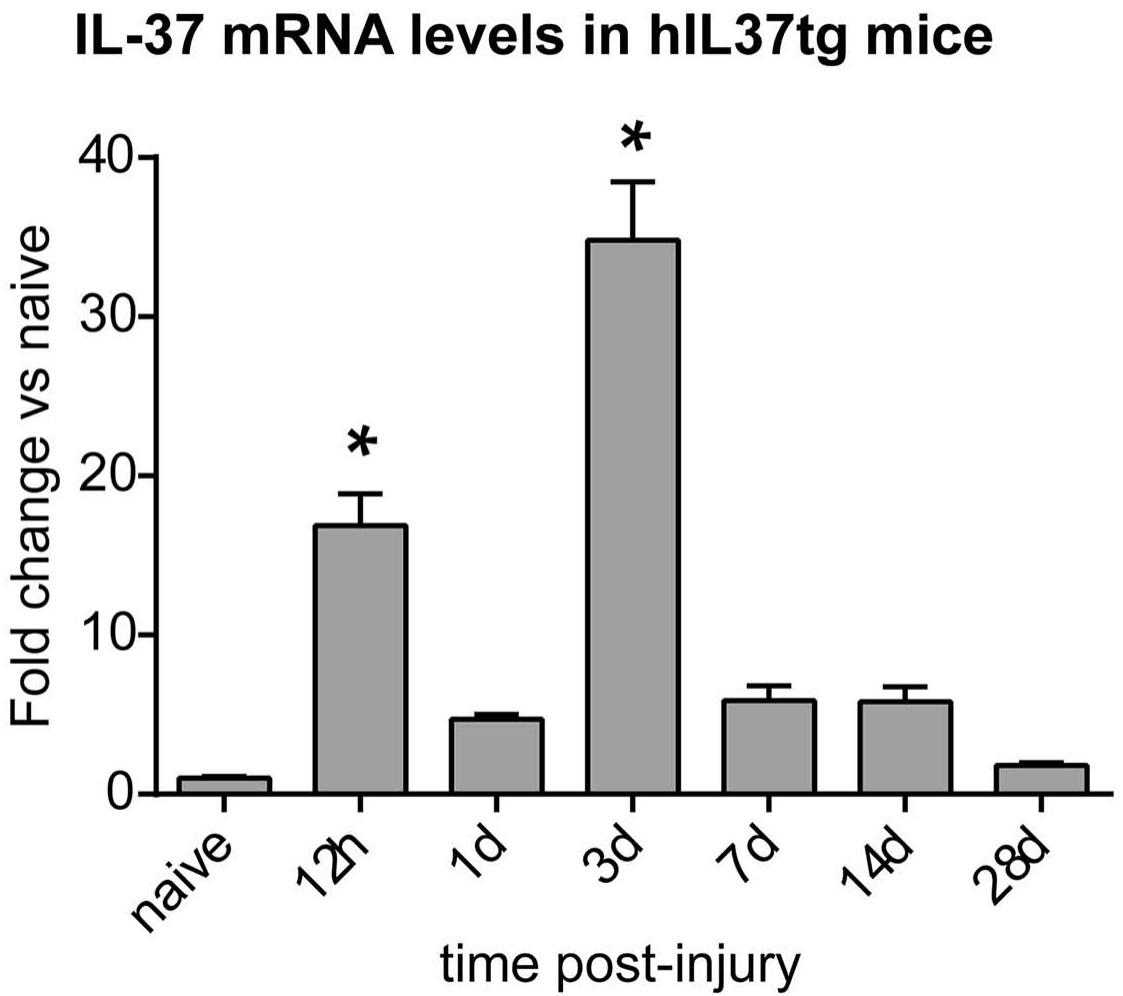
IL-37 mRNA levels in hIL37tg mice
Fold change vs naive
40
30
20
10
0
*
*
naive
12h
1d
3d
7d
14d
28d
time post-injury

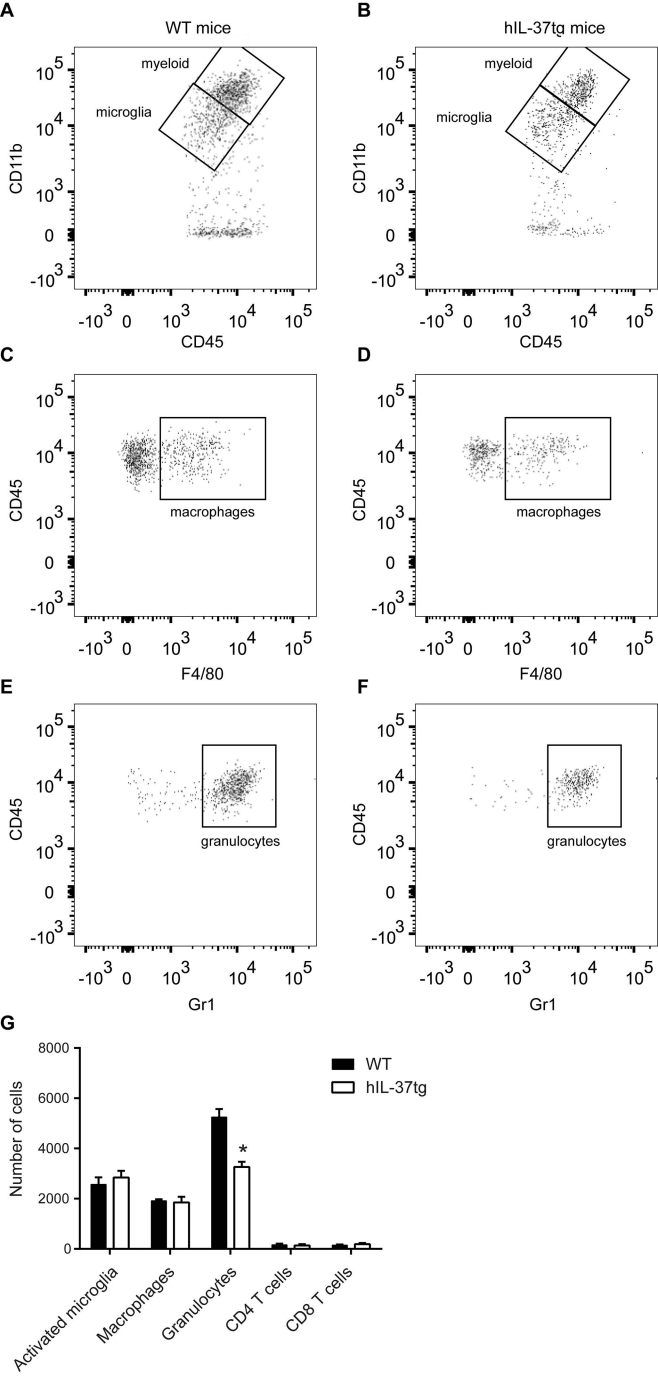
A
WT mice
myeloid
microglia
CD11b
CD45
B
hIL-37tg mice
myeloid
microglia
CD11b
CD45
C
macrophages
CD45
F4/80
D
macrophages
CD45
F4/80
E
granulocytes
CD45
Gr1
F
granulocytes
CD45
Gr1
G
WT
hIL-37tg
Number of cells
8000
6000
4000
2000
0
*
Activated microglia
Macrophages
Granulocytes
CD4 T cells
CD8 T cells

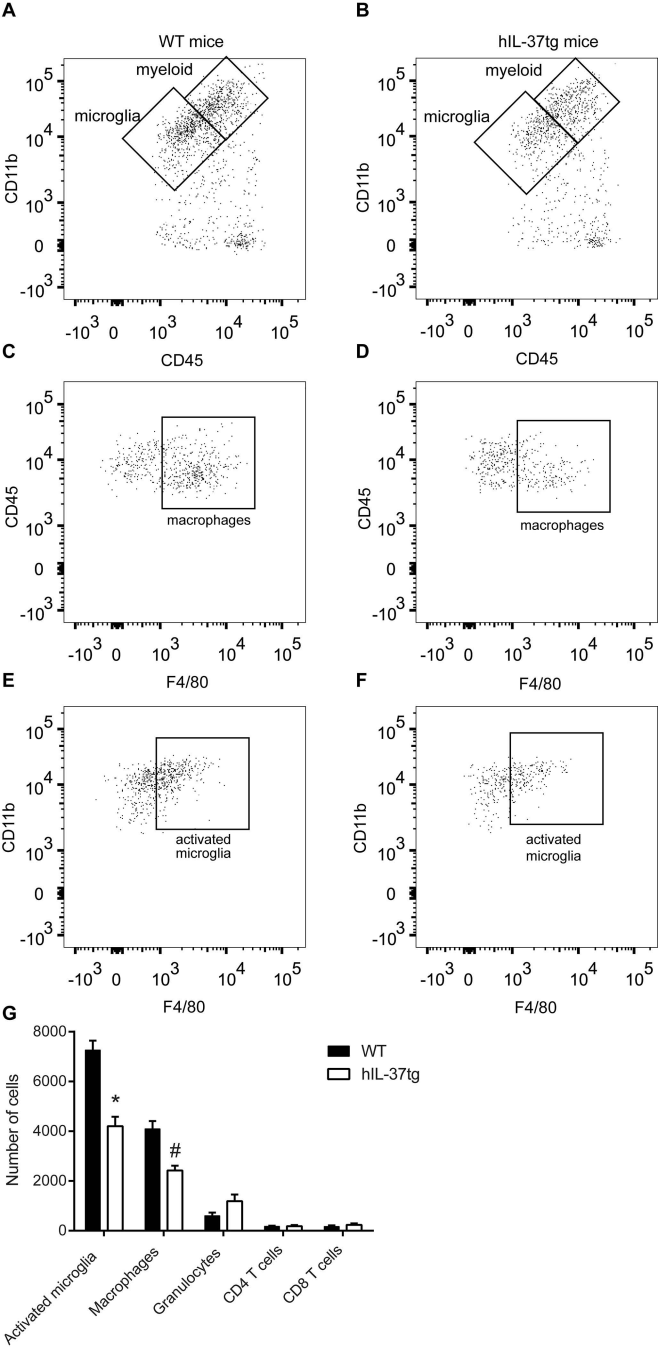
A
WT mice
myeloid
microglia
CD11b
B
hIL-37tg mice
myeloid
microglia
CD11b
C
CD45
macrophages
CD45
F4/80
D
CD45
macrophages
CD45
F4/80
E
activated microglia
CD11b
F4/80
F
activated microglia
CD11b
F4/80
G
WT
hIL-37tg
Number of cells
8000
6000
4000
2000
0
*
#
Activated microglia
Macrophages
Granulocytes
CD4 T cells
CD8 T cells

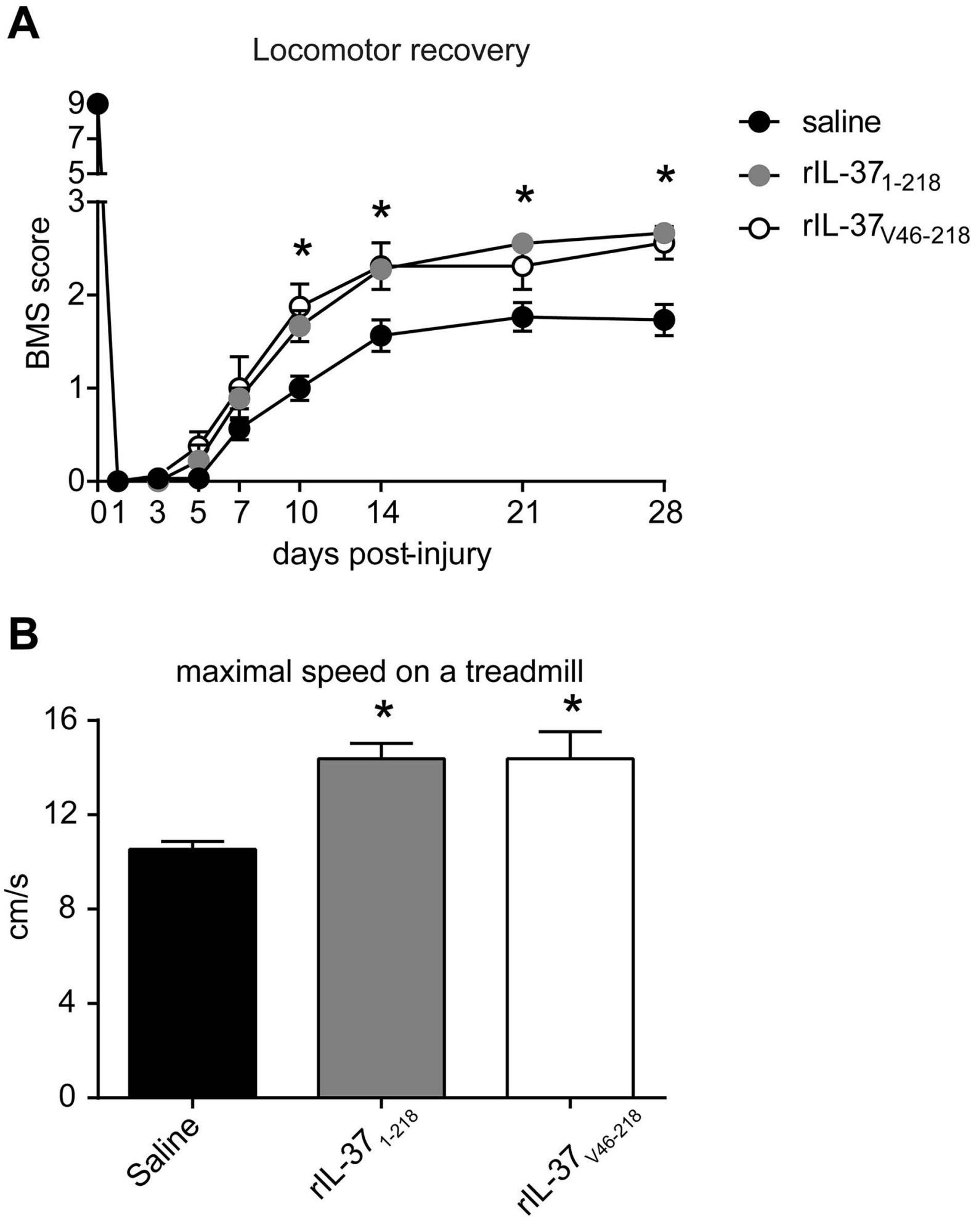
A
Locomotor recovery
BMS score
9
7
5
3
2
1
0
0 1 3 5 7 10 14 21 28
days post-injury
*
*
*
*
saline
rIL-37 1-218
rIL-37 V46-218
B
maximal speed on a treadmill
cm/s
16
12
8
4
0
*
*
Saline
rIL-37 1-218
rIL-37 V46-218

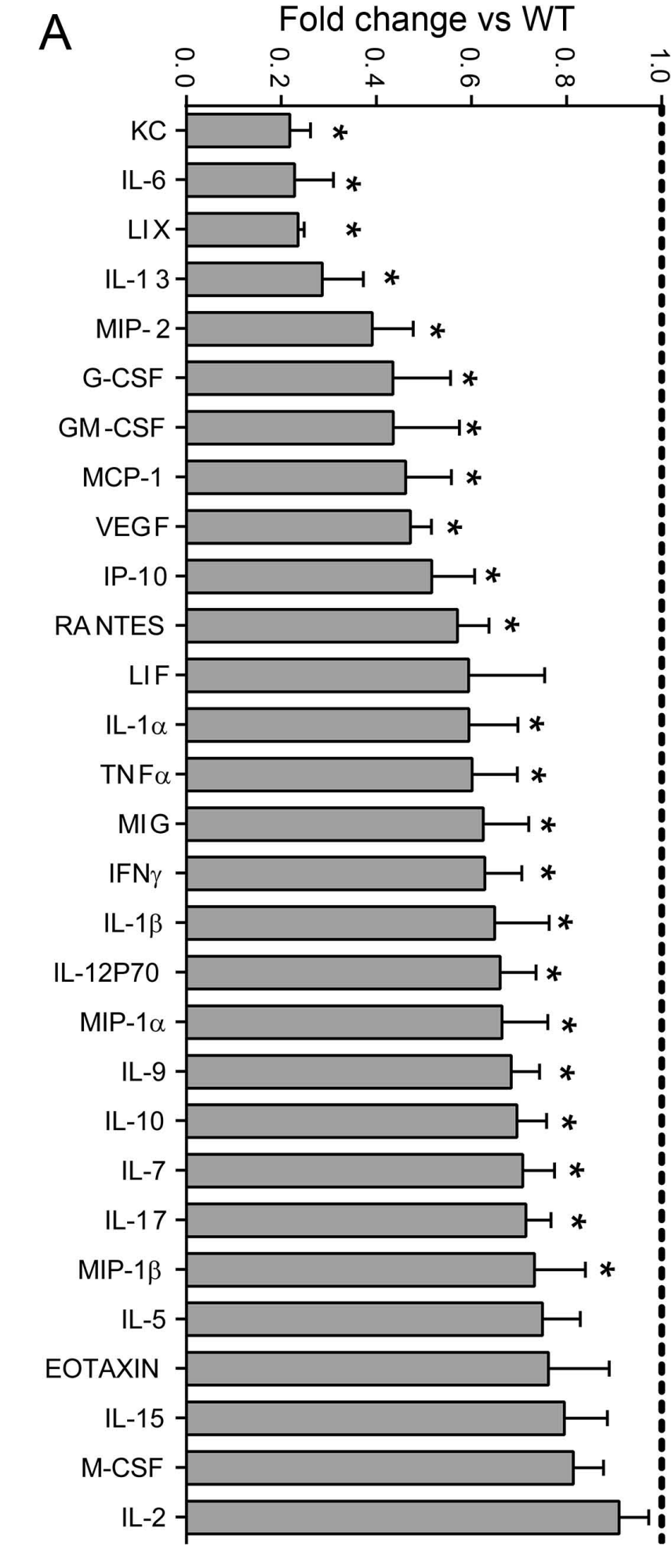
A
Fold change vs WT
0.0
0.2
0.4
0.6
0.8
1.0
KC
IL-6
LIX
IL-13
MIP-2
G-CSF
GM-CSF
MCP-1
VEGF
IP-10
RANTES
LIF
IL-1α
TNFα
MIG
IFNγ
IL-1β
IL-12P70
MIP-1α
IL-9
IL-10
IL-7
IL-17
MIP-1β
IL-5
EOTAXIN
IL-15
M-CSF
IL-2

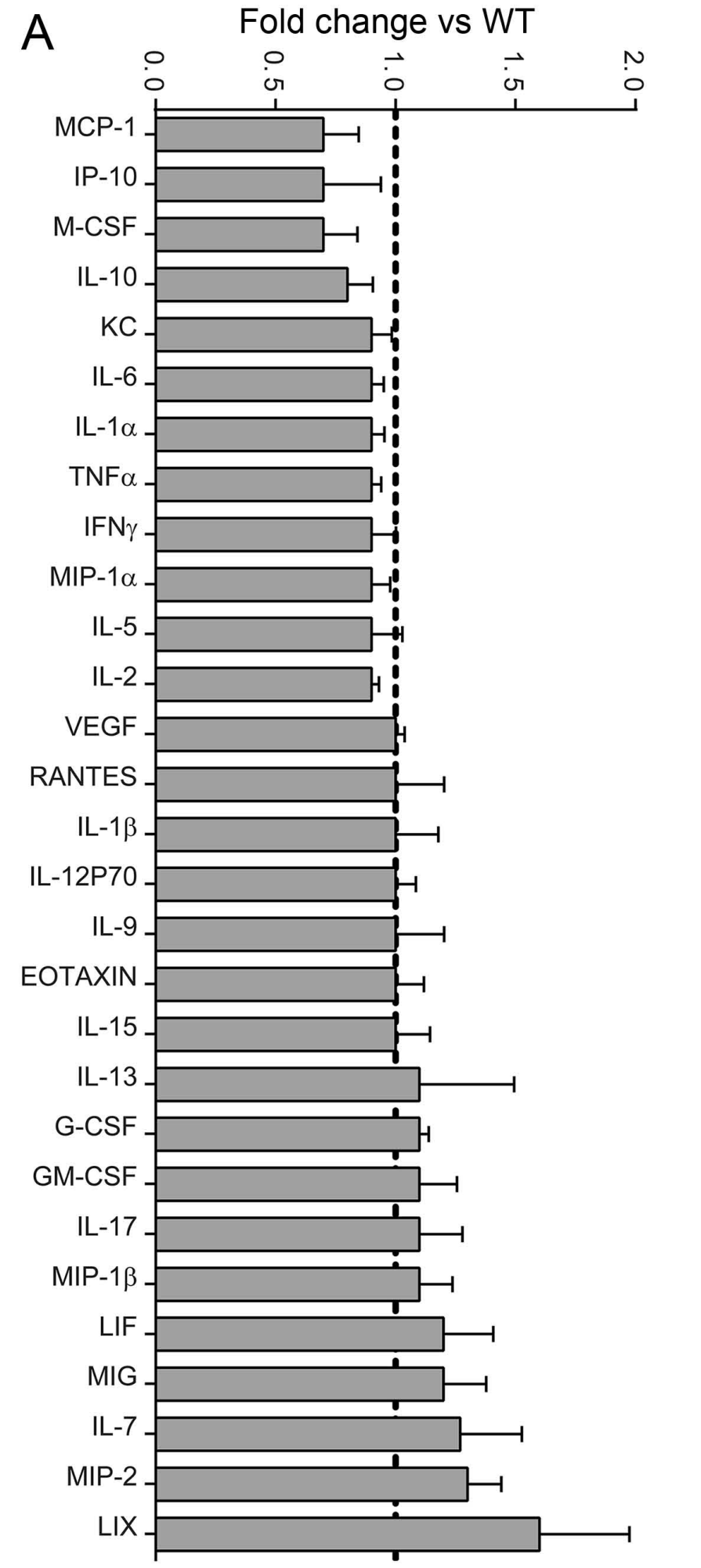
A
Fold change vs WT
0.0
0.5
1.0
1.5
2.0
MCP-1
IP-10
M-CSF
IL-10
KC
IL-6
IL-1α
TNFα
IFNγ
MIP-1α
IL-5
IL-2
VEGF
RANTES
IL-1β
IL-12P70
IL-9
EOTAXIN
IL-15
IL-13
G-CSF
GM-CSF
IL-17
MIP-1β
LIF
MIG
IL-7
MIP-2
LIX